Journal of Structural Biology 167 (2009) 36–46

Contents lists available at ScienceDirect

Journal of Structural Biology

journal homepage: www.elsevier.com/locate/yjsbi

Sequence-specific physical properties of African green monkey alpha-satellite DNA contribute to centromeric heterochromatin formation

Malte Bussiek [a,*], Christian Hoischen [b], Stephan Diekmann [b], Martin L. Bennink [a,*]

[a] Dept. Biophysical Engineering, Faculty of Science and Technology and Mesa+ Institute for Nanotechnology, University of Twente, PO Box 217, 7500 AE Enschede, The Netherlands
[b] Dept. Molecular Biology, Leibniz Institute for Age Research, Fritz-Lipmann-Institute, Jena, Germany

ARTICLE INFO

Article history:
Received 19 December 2008
Received in revised form 6 March 2009
Accepted 18 March 2009
Available online 28 March 2009

Keywords:
Alpha-satellite DNA
Centromere
Chromatin
Atomic force microscopy
Optical tweezers

ABSTRACT

Satellite DNA, a major component of eukaryotic centromeric heterochromatin, is potentially associated with the processes ensuring the faithful segregation of the genetic material during cell division. Structural properties of alpha-satellite DNA (AS) from African green monkey (AGM) were studied. Atomic force microscopy imaging showed smaller end-to-end distances of AS fragments than would be expected for the persistence length of random sequence DNA. The apparent persistence length of the AS was determined as 35 nm. Gel-electrophoresis indicated only a weak contribution of intrinsic curvature to the DNA conformations suggesting an additional contribution of an elevated bending flexibility to the reduced end-to-end distances. Next, the force-extension behavior of the naked AS and in complex with nucleosomes was studied using optical tweezers. The naked AS showed a reduced overstretching transition force (−18% the value determined for random DNA) and higher forces required to straighten the DNA. Finally, reconstituted AS nucleosomes disrupted at significantly higher forces as compared with random DNA nucleosomes which is probably due to structural properties of the AS which stabilize the nucleosomes. The data support that the AS plays a role in the formation of centromeric heterochromatin due to specific structural properties and suggest that a relatively higher mechanical stability of nucleosomes is important in AGM–AS chromatin.

1. Introduction

The faithful segregation of the genetic material into daughter cells during mitosis and meiosis is ensured by the centromeres. These are the chromosomal loci where the kinetochores – multiprotein complexes serving as attachment sites for the spindle apparatus – are organized. It is not clear which factors determine the centromeric locus in the chromosomes of higher eukaryotes. The centromere position is not strictly dependent on a primary DNA sequence (Amor and Choo, 2002). It is probably determined by the centromeric chromatin structure which is characterized by distinct features with respect to the chromatin in chromosome arms (Canapa et al., 2002; Henikoff and Dalal, 2005; Dalal et al., 2007; Conde e Silva et al., 2007; Folco et al., 2008). Centromeres are typically embedded in the highly condensed heterochromatin which mainly forms on large arrays of tandemly repeated DNA sequences, referred to as satellite DNA. The hypothesis is that satellite DNA facilitates heterochromatin formation by sequence-dependent physical properties. A-tract induced permanent curvature is a property of satellites in numerous species (Martinez-Balbas et al., 1990; Fitzgerald et al., 1994). A specific pattern of intrinsic bends in satellites may be implicated in the positioning of nucleosomes (Fitzgerald et al., 1994). Nucleosomal phasing along satellite repeats is expected to promote the condensation of chromatin fibers (Gilbert and Allan, 2001). In addition to the positioning of nucleosomes, their structural stability may be important. This is indicated by the observation that sequences with the highest affinities for nucleosome formation localize to centromeres in yeast and mouse (Widlund et al., 1997; Segal et al., 2006).

Alpha-satellite DNA (AS)[1] is the primate specific type of centromeric repetitive DNA with a monomer length of ~171 bp. AS can be grouped into an old and a new sequence type. The new type is found only in higher primates. Centromeric AS-arrays in higher primates are composed of divergent AS monomers organized into complex higher order repeat structures (Alexandrov et al., 2001). A subset of the new type AS monomers contains the CENP-B box, the binding sites for the kinetochore protein CENP-B. Satellite arrays with CENP-B boxes, but not without, are capable of *de novo* centromere formation (Harrington et al., 1997; Okada et al., 2007). CENP-B may have a structural function relating to the organization of chromatin, e.g. it may set nucleosomal positions within the satellite repeats (Tanaka et al., 2005). The African green monkey (AGM) (*Cercopithecus*

* Corresponding authors. Fax: +31 53 4891105.
E-mail addresses: m.bussiek@utwente.nl, m.bussiek@web.de (M. Bussiek), m.l.bennink@utwente.nl (M.L. Bennink).

[1] *Abbreviations used:* AGM, African green monkey; AS, alpha-satellite DNA.

1047-8477/$ - see front matter © 2009 Elsevier Inc. All rights reserved.
doi:10.1016/j.jsb.2009.03.010

aethiops) harbors the old type which is characterized by a homogeneous monomeric organization and by the absence of the Cenp-B box (Goldberg et al., 1996; Alexandrov et al., 2001). Especially because of the homogeneity of the AS-arrays in AGM, it is very important to find out if here the AS could be involved in the heterochromatin formation. It is known that nucleosomes are positioned along AGM–AS arrays sequence-dependently (Neubauer et al., 1986; Bussiek et al., 2007). Slightly reduced electrophoretic mobility in polyacryl amide gels indicated weak intrinsic curvature (Martinez-Balbas et al., 1990). An A/T rich region in the AGM–AS monomer likely to induce a noticeable bend is located at an end of the major nucleosomal binding site and therefore this region is probably not important for the formation of the majority of the AS nucleosomes (Neubauer et al., 1986; Martinez-Balbas et al., 1990).

The formation of the nucleosome involves substantial deformations of the DNA as it wraps around the histone core (Luger et al., 1997). Therefore, the deformability of DNA and especially the specific pattern of deformable base steps are important for the affinity of certain sequences for the histone proteins (Trifonov and Sussman, 1980; Shrader and Crothers, 1990; Widlund et al., 1999; Widom, 2001; Travers, 2004; Tolstorukov et al., 2007). Many high affinity sequences demonstrate a high bending flexibility as a macroscopic property (Widlund et al., 1999; Cloutier and Widom, 2004; Virstedt et al., 2004). The bending behavior of random sequence DNA is usually described by worm-like-chain (WLC) theory. In this, the persistence length P specifies the length below which the orientation in direction of the DNA persists under thermal fluctuations. Different methods, e.g. cyclization kinetics (Du et al., 2005), high resolution microscopy (Rivetti et al., 1996) or force-extension measurements (Baumann et al., 1997; Wang et al., 1997) yielded apparent persistence lengths P_a of ~50 nm for random DNA in physiological ionic strength. The term 'apparent persistence length' is used since DNA is not a homogenously bending polymer and sequence-induced directional deflections contribute to DNA bending (Bednar et al., 1995; Rivetti et al., 1998; Vologodskaia and Vologodskii, 2002). Increased cyclization rates or decreased end-to-end distances of DNA fragments as compared with the expected values for random DNA would indicate an increased extent of bending. Here, 'the extent of bending' detected by comparing different sequences can be due to the contribution of a different bending flexibility and/or static bending propensity. Atomic force microscopy (AFM) is useful to detect particular bending properties of DNA fragments (Rivetti et al., 1998; Scipioni et al., 2002; Virstedt et al., 2004; Moreno-Herrero et al., 2006). In addition, force-extension measurements using magnetic or optical tweezers reveal different stages of induced deformations in DNA (Cluzel et al., 1996; Smith et al., 1996; Strick et al., 1996; Wang et al., 1997; Cui and Bustamante, 2000; Bennink et al., 2001; 6 Brower-Toland et al., 2002). For random DNA, it has been shown that the persistence length determines the force-extension behavior in the low force regime where the DNA is straightened towards its B-form contour length (Marko and Siggia, 1995; Odijk, 1995; Cluzel et al., 1996; Smith et al., 1996; Strick et al., 1996; Wang et al., 1997). Following straightening, DNA is enthalpically extensible beyond its B-form length at stretching forces between about 10 and 60 pN. This is quantified by the stretch modulus S and included in the extensible WLC (Marko and Siggia, 1995). In a third phase, DNA experiences a highly cooperative disruption of the B-form structure. This is observed as an overstretching by up to ~1.7 times the B-form length without substantially increasing the force further (Smith et al., 1996).

Force-extension measurements were also used to study chromatin: extending chromatin revealed a discontinuous force-extension behavior at forces larger than ~15 pN, indicating the successive disruption of the nucleosomes (Bennink et al., 2001; Brower-Toland et al., 2002; Claudet et al., 2005; Gemmen et al., 2005). The unfolding mechanism of nucleosomes is well characterized (Brower-Toland et al., 2002; Mihardja et al., 2006). Reduced disruption forces due to histone acetylation and histone tail removal were measured using optical tweezers (Brower-Toland et al., 2005).

In this work, conformational properties of naked AGM–AS were studied by gel-electrophoresis and AFM. The question if this DNA forms nucleosomes which are mechanically more stable than nucleosomes formed on random DNA was addressed by force-extension measurements using optical tweezers after reconstitutions of nucleosomal arrays. The optical tweezers were additionally used to extend the naked AS. AFM showed reduced end-to-end distances compared with random DNA. The end-to-end distances translate to P_a = 35 nm. Gel-electrophoresis showed an only weak contribution of intrinsic curvature to the AS conformations suggesting an additional influence by an increased flexibility. The force-extension data qualitatively reproduce a higher extent of bending by higher forces required to straighten the AS, however, analysis with WLC yielded a much lower P_a (18 nm), clearly revealing a deviation from the WLC behavior. The overstretching force was significantly reduced showing a higher susceptibility towards a disruption of the B-form conformation. Forces required to disrupt nucleosomes reconstituted with the AS were higher as compared with nucleosomes reconstituted with plasmid DNA, suggesting that an increased nucleosomal stability is a property of AGM–AS chromatin.

2. Materials and methods

2.1. DNA

Vectors containing a 2-mer and a 13-mer of the 172 bp AGM–AS repeat were prepared previously (Bussiek et al., 2007): an AS 2-mer has been isolated from CV-1 cells after cleavage of the genomic DNA with EcoRI. The 2-mer was cloned in the EcoRI-site of vector pBluescript-II-KS(+) yielding the plasmid pBSα-2. Another fraction of the 2-mer was polymerized to higher repeats. Cloning the ligation product yielded the plasmid pBSα-13 incorporating the AS 13-mer.

pBSα-2 was used for gel-electrophoretic curvature analyses. ~10 μg of the vector was digested with different restriction endonucleases to produce different monomers and fragments incorporating the EcoRI-dimer (Table 1). DNA was purified from enzymes and resuspended in 5 mM Tris, pH 8.5.

For AFM imaging, the AS 6-mer (α-6, 1032 bp) and the 2-mer (α-2, 344 bp) were isolated after a partial digestion of pBSα-13 with EcoRI yielding a distribution of repeat numbers. The fragments were purified from an agarose gel using the Gel Extraction Kit (Qiagen, Hilden, Germany) followed by ethanol precipitation and resuspension in 10 mM Tris, pH 7.5. A control DNA fragment with similar length as the satellite 6-mer was prepared by digestion of pBSα-13 with PvuI and EcoRI. The 1045 bp long PvuI/PvuI DNA fragment, termed rand-1, was isolated from an agarose gel (see Fig. S1 in the Supplementary material).

The complete 13-mer was used for the optical tweezers measurements and chromatin reconstitutions. pBSα-13 was cleaved with XhoI, PstI and BsaI. The 2271 bp XhoI/PstI fragment containing the 13-mer was isolated from an agarose gel. A control DNA was obtained by cleavage of the same plasmid with PstI, PciI and EcoRI and isolation of the 2531 bp PstI/PciI fragment from a gel. Labeling was done by first filling the 3′-recessive XhoI-end of the satellite containing fragment and the PciI-end of the control DNA fragment with dCTP, dGTP, dTTP and dATP-biotin using Klenow(exo-) (New England Biolabs). Excess nucleotides were removed by extensive filtration using Centricon 100 devices. The biotinylated DNA was then ligated with digoxigenin-modified oli-

Table 1
Restriction sites of different enzymes used to produce AGM–AS fragments for the gel-electrophoresis and the determined *k*-factors.

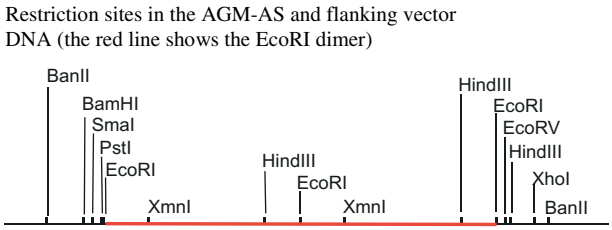

.

	8% PAGE 4 (°C)	8% PAGE 23 (°C)	8% PAGE 100 mM NaCl 23 (°C)	11% PAGE 23 (°C)	8% PAGE 50 (°C)	2% Agarose 23 (°C)
EcoRI	1.07	1.00	1.03	1.04	0.98	0.99
HindIII	1.09	1.04	1.06	1.06	0.99	0.99
XmnI	1.06	1.00	1.00	1.04	0.98	0.97
BanII	1.11	1.08	1.05	1.10	1.02	1.01
EcoRV/PstI	1.12	1.09	1.09	1.14	1.02	0.98
BamHI/XhoI	1.10	1.10	1.06	1.13	1.02	0.99

The error in *k*-factor is ±0.03, as determined from the length standards. EcoRI, HindIII and XmnI produce monomers; BanII, EcoRV/PstI, BamHI/XhoI produce fragments incorporating the EcoRI dimer.

gonucleotides (hybridized from the single stranded oligonucleotides 5′-GCGATCCTGAATGCAGTCTGCA-3′, 5′-GACTGCATTCAGGATCGCdig-3′, Eurogentec) to the PstI-end of the fragments. A 100-fold molar excess of oligonucleotides completely suppressed self-ligation of the target DNA as verified by gel-electrophoresis. The DNA was again purified by extensive centrifugation in Centricon 100. The resulting fragments with ligated oligonucleotides were termed α-13 (2289 bp) and rand-2 (2531 bp, see Fig. S1 in the Supplementary material).

2.2. Curvature analysis

The DNA fragments prepared from pBSα-2 were mixed with loading dye, and analyzed on equilibrated native polyacrylamide gels as outlined previously (Hoischen et al., 2004). Gels were prerun for about 3 h until current and temperature remained constant. Electrophoresis was carried out in 1 × TBE (90 mM Tris–borate, 2 mM Na–EDTA, pH 8.0) at 150 V (8 mA) for approximately 4 h. The temperature was 23 °C (room temperature), or alternatively 4 °C (cold room) or 50 °C (warm oven). After the runs, the gels were stained with ethidium bromide (1 mg/l), followed by rinsing in water prior to documentation. The 1 kb Plus DNA ladder (Invitrogen, Carlsbad, CA, USA) and the 1 kb DNA ladder (New England Biolabs, Ipswich, MA, USA) served as marker fragments together with the intrinsic pBSα-2 fragments resulting from the restriction digestions. Migration of all fragments was determined for each gel and calibration curves were plotted using marker fragments (logarithm of number of base pairs against distance migrated). Apparent size in acryl amide relative to the calibration curve was determined for every anomalously migrating fragment.

2.3. AFM imaging

The DNA prepared for AFM was diluted to concentrations of ~2 nM in 10 mM Tris–Cl, pH 7.5. Mica pre-treated with poly-L-lysine (PL; MW 500–2000, Sigma, Deisenhofen, Germany) was used for DNA immobilization of α-6 and rand-1. The mica was incubated with 20 mg/l PL for 30 s, rinsed with Millipore water and dried under a nitrogen stream. DNA was deposited onto the dried PL-mica for 1 min in buffer supplemented with 100 mM NaCl. α-2 was deposited onto bare mica in buffer supplemented with 10 mM NaCl, 2 mM $MgCl_2$. Mica discs with the bound DNA were washed carefully with 3 ml of Millipore water and dried under a gentle nitrogen stream. Samples were scanned using FESP tips (Veeco) with an AFM setup as described (Van der Werf et al., 1993). Images were acquired at a resolution of 512 × 512 pixels, pixel rate of 3000 Hz at a scan size of 2000 nm.

The recorded AFM images were flattened using SPIP software (version 4.5.1., ImageMetrology, Horsholm, Denmark) and scaled to 1.024 nm per pixel using bilinear interpolation in ImageJ software (version 1.36B, National Institutes of Health, USA). DNA contours were traced using the freehand line tool available in ImageJ. The digitized contours were smoothed by calculating for each coordinate the average of five contiguous points. The contour lengths L_c and end-to-end distances R of the smoothed contours were determined. Only contours with a length within the range defined by the mean plus and minus two times the standard deviation were included. For analysis of the adsorption process of DNA on the PL-mica, the contours of α-6 and rand-1 were divided into segments of varying length L_{seg}. The starting and end positions of the segments were defined using software written in Labview (version 8.2). The starting positions were shifted in 10 nm steps along the entire smoothed contours and corresponded to the *xy*-coordinate where the distance along the contour is closest to 10 nm with respect to the previous point (with a resulting step length variation <0.5 nm). The end-point of each segment with the specified length L_{seg} was defined accordingly relative to each starting point. R was measured for every segment and averaged over all segments generated in the sample.

2.4. Reconstitution of nucleosomal arrays

Histone proteins were isolated from chicken erythrocytes (Simon and Felsenfeld, 1979). SDS–PAGE (15%) verified the equal stoichiometry and purity of the four histones. Recombinant yeast nucleosome assembly protein with a his-tag (yNAP) was prepared after expression from a pET vector made available by F. Clapier and purification using Ni–NTA medium (Qiagen, Hilden, Germany) (Wagner et al., 2005). DNA (linear fragments α-13 and rand-2 or the native supercoiled plasmid pBSα-13) at a final concentration of 17 ng/μl were used for nucleosomal array reconstitutions. First, 8.5–14 ng/μl histone octamers (present in 10 mM Tris–Cl, pH 7.7, 2 M NaCl) were mixed with 67 ng/μl of yNAP-1 (final concentrations) in 100 mM NaCl. After incubation for 20 min at 37 °C, DNA was added and the mixture was kept at 37 °C for another 20 min. Then, reactions were stored at 0 °C and used for measurements within two days. Nucleosome formation was controlled by topoisomer counting. The supercoiled plasmid pBSα-13 reconstituted

with histones was relaxed with topoisomerase I (Promega, Madison, WI, USA) at 37 °C for 2 h, then isolated from all proteins with phenol/chloroform/isoamylalcohol and precipitated with ethanol. The DNA was analyzed on 1.2% agarose gels run in 1 × TBE followed by staining with ethidium bromide. The topoisomer bands were quantified using the gel analysis option in ImageJ.

2.5. Optical tweezers measurements

Stretching experiments were performed using a setup described earlier (Bennink et al., 2001). The DNA tether is built between an optically trapped bead and a bead attached to a micropipette. The micropipette which is fixed in the observation chamber is moved relative to the optical trap using a linearized stage (P-561.3CD, Physik Instrumente, Karlsruhe, Germany) to extend the DNA.

Streptavidin (SA) coated beads with a nominal diameter of 2.67 μm (Bangs Laboratories, Inc., Fishers, USA) at a final concentration of 0.001% (w/v) were mixed with labeled DNA, either naked or reconstituted with histones, at a final concentration of ~0.005 OD_{260} under rotation for several hours in phosphate buffered saline, 0.05% BSA at 4 °C. The SA-beads were diluted 50-fold in 10 mM Tris–Cl, pH 7.5, 0.05% BSA, 100 mM NaCl before introducing them into the observation chamber filled with the same buffer. Protein G coated beads with nominal diameter of 2.1 μm (Bangs Laboratories) were modified with anti-digoxigenin and also diluted to the appropriate concentration. An anti-digoxigenin modified bead was first trapped in the laser focus and attached to the micropipette. Then, a SA-bead with bound DNA was trapped in the laser focus. The bead at the micropipette was approached to the bead in the optical trap to bind the digoxigenin modified end of the DNA. In the measurements of naked DNA, binding was tested before recording a force-extension curve by carefully moving the stage. Measurements of chromatin were 'blindly' started immediately after a short approach of the beads to prevent damage of the chromatin complexes.

Force-extension curves were recorded at stage velocities between 50 and 500 nm/s. The trap stiffness was ~400 pN/μm and was determined using the power spectrum method (Gittes and Schmidt, 1998). Multiple power spectra were recorded for every bead and corrected for the limited band-width of the photo detector (Huisstede et al., 2006). Both, the displacement of the optically trapped bead from the trap center due to stretching forces and the distance between beads were evaluated by analyzing microscopic images acquired at a rate of 25 Hz during a measurement. Since the microscopic images of the two beads interfere when they are in a close proximity, bead positions were determined from sections of the bead's circumferences that face away from each other. Software written in Labview (version 8.2) was used to detect the *x*-position of the outer sections by adding the gray values from multiple (~20) line scans. A Gaussian function was fitted to the detected 'outer' peaks from the summed line scans to determine the positions at sub-pixel resolution (pixel size was 60 nm). This measurement yielded the relative change in bead positions and distance between them. The starting extension was determined by measuring distances along one-pixel lines passing through the bead centers at distances large enough that the images showed two beads that were clearly separated. The zero-force position of the optically trapped bead corresponded to its mean position during the stage movement back to the starting position after the disruption of the DNA tether.

3. Results

3.1. Gel-electrophoresis shows a weak gel retardation of AGM–AS fragments

Intrinsic curvature of DNA can be identified by a retarded migration in polyacrylamide gels. The *k*-factor is the observed apparent fragment length divided by the known length (in bp). Curvature variation in normal DNA sequences is between *k*-factors of 0.98 and 1.05. Strong curvature induced by A_n-tracts (with $n \geqslant 4$) arranged in phase with the helical turns can result in *k*-factors ⩾2.0 (Diekmann, 1986; Koo and Crothers, 1988).

The studied AGM–AS sequence is shown in Fig. 1. Like satellite DNA of many other species, the AGM–AS is A/T rich (57%) and contains tracts of homopolymeric A/T nucleotides. These are predominantly not arranged in phase with the helical turns and mostly contain only three consecutive A/T. Two tracts with four or five consecutive A/T are separated by two helical turns and have nearly the same helical position (between sequence positions 138 and 164). A *k*-factor of 1.08 for the HindIII-monomer (positions 1–172 in Fig. 1) has been measured at 4 °C in 7% acryl amide (Martinez-Balbas et al., 1990). We were interested in an extended analysis using varying electrophoresis conditions as well as different monomers and the EcoRI-dimer which incorporates the known major nucleosomal binding site uninterrupted (Neubauer et al., 1986) (see Table 1). As can be seen in Table 1, all monomer length fragments, including the HindIII-monomer, did not show any appreciable gel-retardation under standard conditions (23 °C, TBE buffer). A weak retardation of the fragments containing the dimer was noticed. At more stringent conditions, i.e. at a reduced temper-

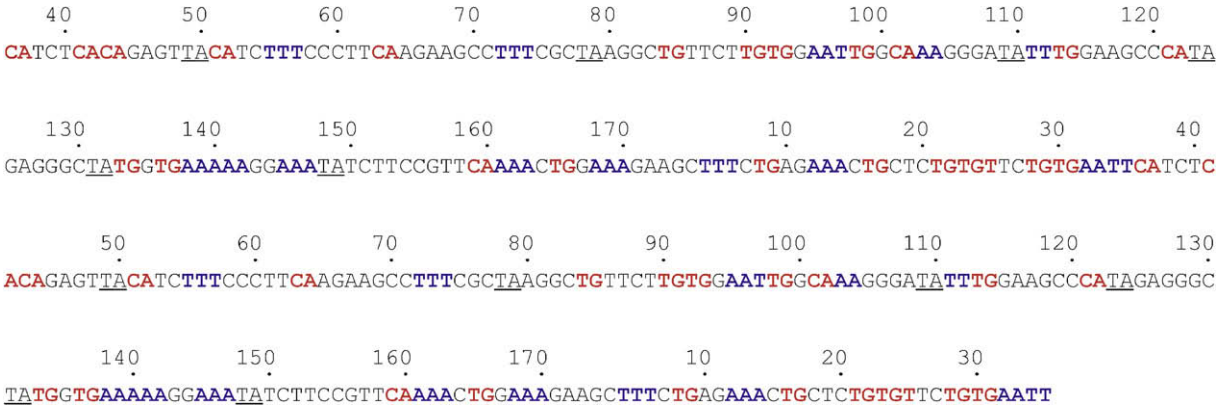

Fig. 1. DNA sequence of the isolated AGM–AS (Bussiek et al., 2007). Shown is the EcoRI-2-mer with sequence numbering according to Rosenberg et al. (1978). Highlighted sequence portions (blue, A/T tracts with ⩾3 successive A/T; red, CA/TG steps and underlined, TA steps) are addressed in the main text. The known most preferred nucleosomal binding site ranges from sequence positions 142 to 114 (Neubauer et al., 1986).

ature or increased acryl amide concentration, *k*-factors for all fragments increased slightly. This increase is expected for intrinsic curvature, although here the differences were small (Diekmann, 1987; Hoischen et al., 2004). As well expected is the absence of retardation at increased temperature or in the agarose gel. The published *k*-factor for the HindIII-monomer (Martinez-Balbas et al., 1990) agrees well with our measurement at 4 °C in 8% acryl amide ($k = 1.09$). However, considering all fragments, the retardation was essentially absent in the presence of 100 mM NaCl suggesting that the effect of intrinsic bends is overruled by thermal fluctuations under these conditions. Although this analysis shows some secondary structure, it confirms that AGM–AS is not substantially curved.

3.2. AFM-imaging of naked AGM–AS conformations

AFM was used to characterize conformational properties of AGM–AS based on measurements of the end-to-end distance *R* of the imaged DNA fragments. The 1032 bp long satellite 6-mer (α-6) and the 1045 bp long plasmid DNA fragment rand-1 were compared. Additionally the satellite 2-mer (α-2) was imaged. The question of distinct bending properties is addressed by comparison with the expected end-to-end distances for random DNA. The expected mean squared end-to-end distance $\langle R^2 \rangle$ for random DNA in free solution can be calculated assuming $P_a = 50$ nm by

$$\langle R^2 \rangle_{3D} = 2P_aL_c\left[1 - \frac{P_a}{L_c}\left(1 - e^{-\frac{L_c}{P_a}}\right)\right]. \quad (1)$$

DNA can be bound to mica in an appropriate buffer such that it behaves as a 2-dimensional WLC and in this case P_a in Eq. (1) has to be multiplied by two yielding (Rivetti et al., 1996).

$$\langle R^2 \rangle_{2D} = 4P_aL_c\left[1 - \frac{2P_a}{L_c}\left(1 - e^{-\frac{L_c}{2P_a}}\right)\right]. \quad (2)$$

P_a can also be verified by irreversibly trapping the DNA on pre-treated mica, for example by using mica treated with poly-L-lysine (PL) (Bussiek et al., 2003). Then, $\langle R^2 \rangle$ results from an orthogonal projection onto a plane (Rivetti et al., 1996):

$$\langle R^2 \rangle_{proj} = \frac{2}{3}\langle R^2 \rangle_{3D}. \quad (3)$$

In the trapping method, the DNA preserves the characteristics of the 3D conformation. We use this method to minimize a possible influence by excluded volume effects which would increase $\langle R^2 \rangle$. Excluded volume effects are particularly strong in 2D-equilibrated

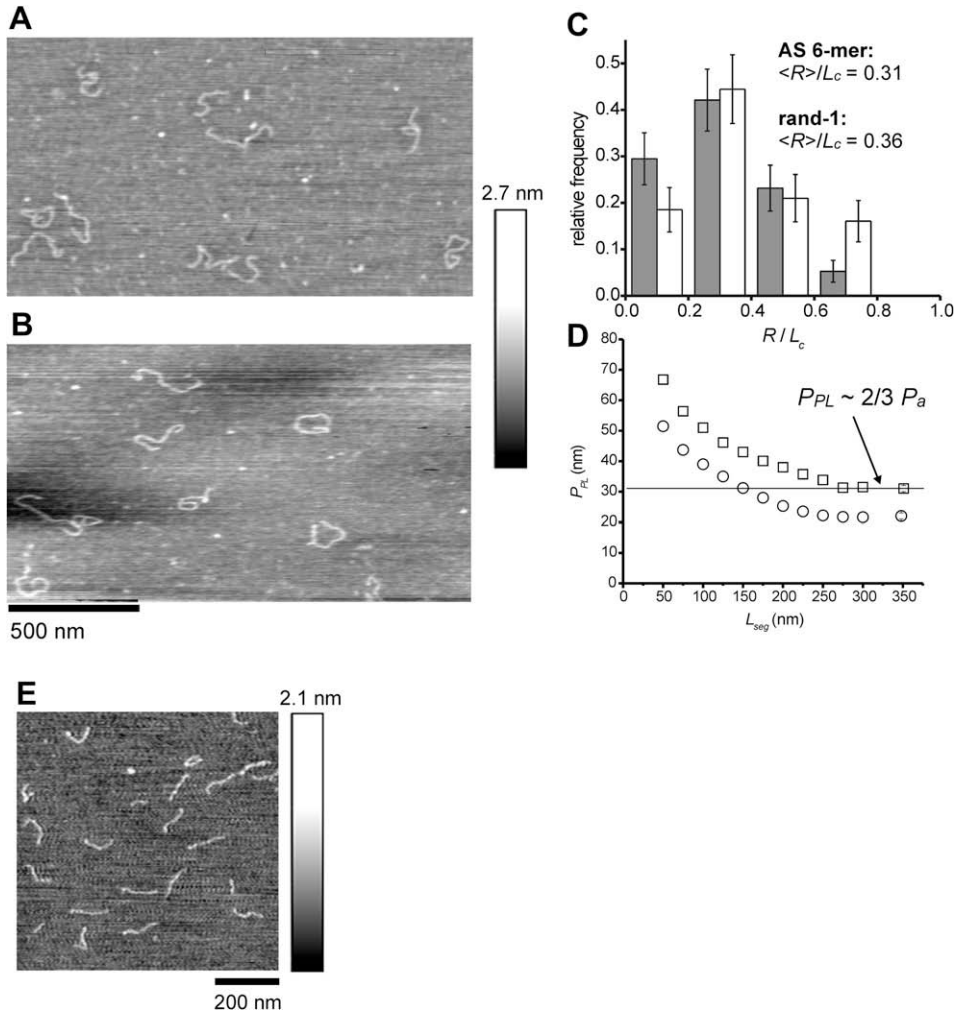

Fig. 2. AFM imaging and analysis of AGM–AS. (A) Tapping mode AFM image of AS 6-mers, α-6 (A) and the plasmid DNA fragment, rand 1 (B) adsorbed in buffer supplemented with 100 mM NaCl to mica coated with poly-L-lysine (PL). (B) Distribution of end-to-end distances *R* of α-6 (gray bars) compared with the distribution for rand-1 (white bars). (D) Uncorrected persistence length P_{PL} calculated as a function of DNA segment length L_{seg} for rand-1 (squares) and α-6 (circles). P_{PL} refers to a calculation without considering the surface adsorption (Eq. (1)). This is assumed here for better presentation because using Eq. (3) would yield extremely high persistence lengths at small segment lengths. The last data point for both DNAs corresponds to the entire fragment ($L_{seg} = L_c$). The horizontal line indicates P_{PL} for the entire rand-1 with a value expected for trapping and $P_a = 50$ nm. (E) AFM image of AS 2-mers adsorbed in buffer supplemented with 10 mM NaCl, 2 mM $MgCl_2$ to bare mica.

Table 2
Characterization of DNA fragments imaged by AFM.

Fragment	L_{exp} (nm)	L_c (nm)	$\langle R^2 \rangle$ (nm^2)	P_a (nm)[a]	(Model)	Surface	n
rand-1	355	351 ± 9	20,040	50 ± 1	(Eq. (3))	PL-mica	87
α-6	351	348 ± 8	14,050	35 ± 1	(Eq. (3))	PL-mica	91
α-2	117	113 ± 6	7940	35 ± 8	(Eq. (2))	bare mica	81

L_{exp}, expected contour length for 0.34 nm/bp; n, number of molecules.
[a] P_a was calculated on the basis of the measured contour length L_c. The error in P_a was estimated on the basis of the standard deviation of L_c.

conformations as compared with the 3D-conformations. They depend on the DNA length as well as on the bending properties (Rivetti et al., 1996). Fig. 2A and B shows AFM images of α-6 and rand-1, respectively, adsorbed to PL-mica in the presence of 100 mM NaCl and scanned in air. For all DNAs, the measured lengths were slightly below the expected L_c (Table 2), a typical observation in AFM studies of DNA (Rivetti et al., 1996; Bussiek et al., 2003). The end-to-end distance distribution of α-6 is shifted to smaller values compared with that of rand-1 (Fig. 2C). This shows that the conformations of the satellite DNA were more compact on average.

$\langle R^2 \rangle$ measured for the plasmid DNA fragment (rand-1) corresponds with expectation for $P_a = 50$ nm under the assumption of the orthogonal projection (Eq. (3)) (Table 2). This was expected for the PL concentration used to modify the mica (Bussiek et al., 2003). $\langle R \rangle / L_c$ measured for α-6 (Fig. 2C) is 14% smaller than would be expected for $P_a = 50$ nm. Applying WLC to α-6 yields $P_a = 35$ (±∼1) nm based on the measured $\langle R^2 \rangle$. We use the persistence length to further analyze the trapping mechanism and to find out if both DNAs are similarly influenced by the surface adsorption. For this, the apparent persistence length was evaluated for segments with varied lengths L_{seg} of the entire fragments (see Section 2). To observe a dependency of the persistence length on the segment length, the specific adsorption model is irrelevant but it is useful for presentation to assume Eq. (1) (see caption to Fig. 2). This calculated persistence length was named P_{PL}. Fig. 2D shows that P_{PL} increased with decreasing L_{seg} for both DNAs. This was expected, because the simple orthogonal flattening should be prevented locally due to the DNA stiffness and surface re-arrangements of shorter segments are possible (Bussiek et al., 2003). Both these factors increase $\langle R \rangle$. A corresponding behavior has been observed for trapped vimentin filaments (Mucke et al., 2004). P_{PL} approached the values for the entire fragments above about 250 nm (this value is about 2/3 P_a). This proofs that the orthogonal projection can be assumed to determine P_a for the DNA lengths of the molecules studied here (Mucke et al., 2004). It is interesting to note that the persistence lengths are different between α-6 and rand-1 for all segment lengths, showing as well a clear difference in the bending properties on smaller length scales (Fig. 2D). To analyze quantitatively a shorter length, the 2-mer (α-2) was bound to bare mica in buffer containing 10 mM NaCl and 2 mM $MgCl_2$ (Fig. 2E). The ability for a 2D-equilibration is well known under these conditions (Rivetti et al., 1996; Bussiek et al., 2003; Virstedt et al., 2004). $\langle R^2 \rangle$ measured for this fragment as well yields $P_a = 35$ nm, here using the 2D-equilibration model (Eq. (2)). An evaluation of P_a for shorter segments of the 2-mer was not reliable because of the limited resolution combined with the fact that large changes in P_a correspond with only small changes in $\langle R \rangle$ at short contour lengths. However, it was conceivable that a single restricted region is responsible for the reduced end-to-end distances and that this would be recognized by comparing segments of the imaged α-2 contours. A centered bend in a DNA fragment causes stronger reduced end-to-end distances than a bend located closer to an end (Rivetti et al., 1998). Dividing each α-2 contour into two equal parts (corresponding with the EcoRI-monomer) gave $\langle R \rangle = 50$ nm ($P_a = 38$ nm) in which the data for both halves were combined. Then, the segment starting halfway the first monomer and ending halfway the second monomer of each α-2 contour was analyzed. The starting site would ideally be at sequence position 126 (Fig. 1) and was defined with an accuracy of 10 bp based on the percentile standard deviation of the measured contour length (Table 2). The region containing the two tracts with four or five consecutive A/T mentioned above is near the center of the EcoRI-monomer, but near an end of the segment that is starting at position 126. However, this segment yielded the same mean R. As a result, we were not able to discern a restricted bent region in either of these segments.

The AFM measurements, summarized in Table 2, show that the end-to-end distances of the AS are shorter than is expected for random DNA from WLC. The conclusion is that the AS exhibits a higher extent of bending as compared with random DNA which can be due to increased flexibility and/or a contribution of intrinsic bends. However, the weak gel-retardation, which was especially not clearly detectable in the presence of 100 mM NaCl, suggests that an increased flexibility partly accounts for the small P_a.

3.3. Force-extension measurements

The main goal of force-extension measurements was to characterize the mechanical stability of nucleosomes formed with the AS. The sample DNAs compared were the AS 13-mer (α-13, L_c = 2289 bp or 778 nm) and the plasmid DNA fragment rand-2 (L_c = 2531 bp or 860 nm). Both DNAs were labeled with digoxigenin on one end and with biotin on the other end to suspend them between two microbeads modified with either anti-digoxigenin or streptavidin. In addition to the measurements of nucleosomal arrays, we used the DNA-constructs to study the force-extension behavior of the naked AS.

3.3.1. Naked AGM–AS shows a distinct force-extension behavior

Fig. 3A shows examples of the obtained force-extension curves revealing the typical profiles of naked DNA. A noticeable feature in the data for α-13 is a clearly lower overstretching transition force than for rand-2. The overstretching force for rand-2 is in good agreement with previous measurements of random sequence DNA (Smith et al., 1996; Baumann et al., 1997; Bennink et al., 2001). Unlike the measurement in Fig. 3, which is done at a pulling velocity of 200 nm/s, the DNA tethers usually ruptured before reaching the overstretching plateau. This is most likely due to rupturing the digoxigenin–anti-digoxigenin bond. To repeatedly observe the overstretching plateau the pulling speed was increased to 500 nm/s in a separate set of pulls. On average, the overstretching transition force of α-13 was at 56 (±0.5 SE) pN (n = 13) which is 18% smaller than the value for rand-2 measured at 68 (±1.4 SE) pN (n = 9). The forces were read in the initial region where the curve has turned into the plateau because the full plateau length was not always available. The lower transition force demonstrates that AGM–AS is more susceptible towards a disruption of the B-form DNA conformation.

The AGM–AS is additionally distinguished from random DNA by its force-extension behavior in the low force regime. Straightening *random* DNA towards the B-form contour length is described by the

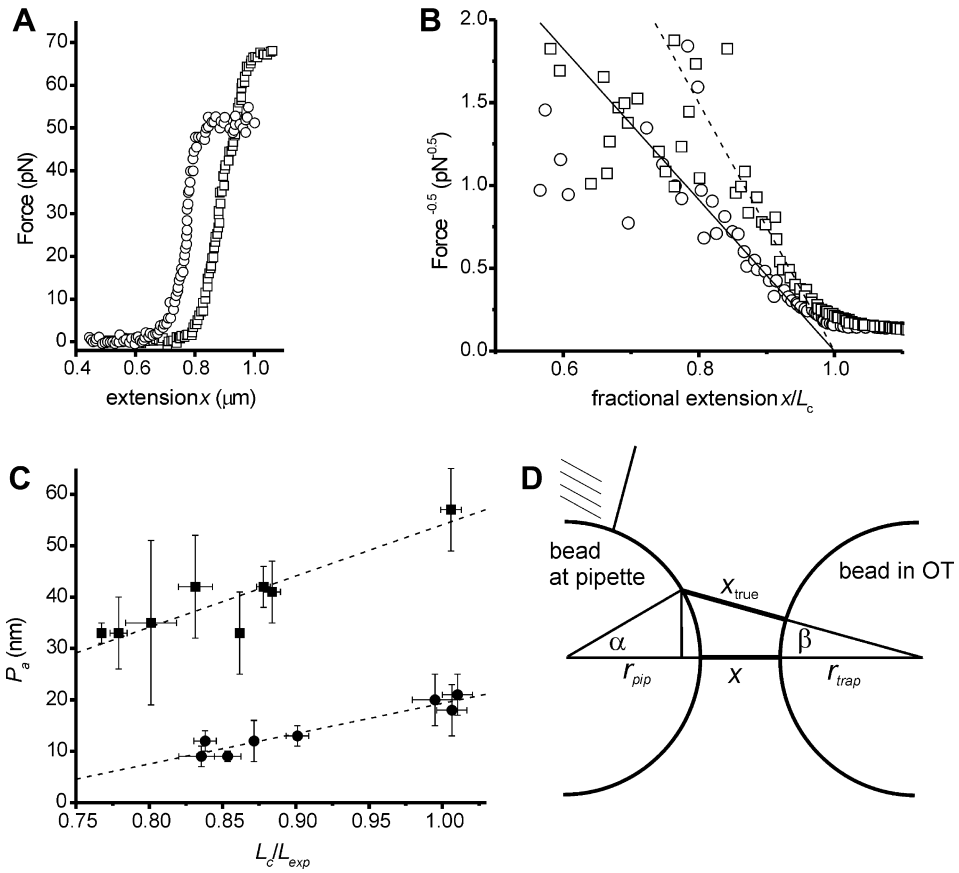

Fig. 3. Force-extension measurements of AS 13-mer α-13 (circles) and plasmid DNA fragment rand-2 (squares). (A) Force-extension curves recorded at a pulling speed of 200 nm/s. (B) Analysis of the low force regime. The data are the same as in Fig. 3A with normalized extensions (expected contour lengths L_{exp} are 860 nm for rand-2 and 778 nm for α-13). A linear relationship between $F^{-0.5}$ and extension x is obtained for fractional extensions ~0.85–0.95. The lines are linear fits to data points in this range of extensions (the strongly scattered data points at lower fractional extensions are not considered). Using Eq. (4) yielded P_a = 57 ± 8 nm, L_c = 865 ± 6 nm for the shown example of rand-2 stretching. Applying WLC to the shown curve of α-13 yielded P_a = 20 ± 5 nm, L_c = 774 ± 12 nm. (C) Plot of observed P_a versus L_c for individual force-extension curves. The lines are linear regressions with correlation coefficients >0.9. (D) Geometry of DNA tethers. The attachment point of the DNA at the micropipette bead is specified by the angle α. β is the rotation angle of the optically trapped bead at a given extension. r_{pip} is the radius of the bead at the micropipette and r_{trap} the radius of the optically trapped bead. x is the apparent extension (the observable space between beads) and x_{true} the real end-to-end distance of the DNA. For this idealized configuration, x can be expressed as follows: $x = \sqrt{(x_{true} + r_{pip})^2 - (\sin \alpha r_{pip})^2} - (r_{pip} - \cos \alpha r_{pip}) - r_{trap}$.

inextensible WLC for forces up to ~10 pN. A strong stretching WLC behavior is obtained at fractional extensions between ~0.85 and 0.95 which is described by (Odijk, 1995)

$$\frac{x}{L_c} = 1 - \frac{1}{2}\left(\frac{kT}{FP_a}\right)^{0.5}, \quad (4)$$

where k is the Boltzmann's constant, T the temperature and x the extension. Fig. 3B shows the linear change of $F^{-0.5}$ with increasing x in this strong stretching regime for the same curves as in Fig. 3A. Compared with rand-2, the stretching forces for α-13 clearly increased at smaller fractional extensions. Correspondingly, the slopes of the linear fits differ. To verify that the measurements of rand-2 yielded the expected persistence length, L_c and P_a were derived from the linear fits. Here, a first observation was that L_c and P_a showed additional variation. L_c was typically smaller than the expected contour lengths. This can be explained by the fact that the DNA tethers were not well aligned with the direction in which the force is exerted (Fig. 3D). This is due to binding one end of the DNA to a bead fixed at a micropipette. Only the bead in the optical trap is able to rotate freely. In force-extension curves of misaligned tethers the stretching force increases at smaller fractional extensions as compared with curves of aligned tethers. This leads to apparently reduced P_a, depending on the tilt angle of the tether. P_a therefore decreases with decreasing apparent L_c which is well visible in Fig. 3C. To compensate for this influence, force-extension curves yielding reduced L_c were re-calculated assuming the tether geometry in Fig. 3D. The angle α specifying the attachment site of the DNA at the fixed bead was defined on the basis of the ratio between the fitted L_c and the expected contour length. The true extensions were approximated taking into account that the rotation angle β decreases with extension. The obtained corrected force-extension curves were re-analyzed in the same way as shown in Fig. 3B. This gave on average P_a = 54 (±2 SE) nm for rand-2 (n = 8). This mean value corresponds with the P_a read at the intercept between the linear regression and the expected contour length in Fig. 3C (as well 54 nm). This gives sufficient support that the misalignment of the DNA tethers can be accounted for. A correction of the forces by including a displacement of the force measuring bead in the direction orthogonal to the stretching direction was neglected because the effect on the fit result was very small (not shown). The reason for this is that the rotation angle is small at the higher extensions.

We also applied WLC to the force-extension data of the AS. The same analysis as before for rand-2 firstly showed a similar relationship between the fitted L_c and P_a due to the misalignment. Secondly, P_a was consistently smaller than for rand-2 (Fig. 3C). Since the stretching forces for rand-2 were as expected for random DNA, it can be concluded that straightening the AS was reproduc-

ibly associated with higher forces than straightening random sequence DNA. This result is in qualitative agreement with the AFM measurements since higher stretching forces in the low force regime are expected to reflect a higher extent of bending. However, this analysis yielded an unusually low mean P_a of 18 (±1.2 SE) nm ($n = 8$) which is different from P_a derived from the end-to-end distances measured by AFM. This confirms a deviation from the WLC behavior.

The stretch modulus S was derived from the compensated force-extension curves using the extensible WLC (Marko and Siggia, 1995). L_c and P_a derived before were introduced in the extensible WLC as fixed parameters. The stretch modulus was allowed to vary in the fitting algorithm. No significant difference between rand-2 and the AS were detected. The obtained values were 834 (±108 SE) pN for rand-2 ($n = 8$) and 939 (±71 SE) pN for α-13 ($n = 6$). However, it is not clear whether S can be reliably evaluated because WLC theory may not be suitable to describe the different force regimes of the AS, as suggested by the unusually low P_a.

3.3.2. AGM–AS nucleosomes resist higher stretching forces

The force-induced unraveling of nucleosomes reconstituted with α-13 and rand-2 was studied by extending the DNA at a constant pulling speed of 50 nm/s. Nucleosomal arrays were reconstituted employing the preparation method with yeast NAP-1 (McQuibban et al., 1998). This allows a controlled binding of the histone proteins without unspecific aggregation. Reconstitution with NAP-1 yielded positioned nucleosomes on concatemeric 5S rDNA (Leuba et al., 2003). Nucleosome formation was verified by observing their capacity to induce supercoils in circular DNA (Fig. 4). The observed stoichiometry (assuming one nucleosome per supercoil detected as the linking number change) was then used to control the loading of α-13 and rand-2 with nucleosomes. Although this can only give a rough estimate for linear DNA, which is expected to be less loaded than circular DNA, counting the number of supercoils guaranteed that α-13 and rand-2 were not overloaded with histones.

Fig. 5A shows the typical force-extension profiles for unraveling nucleosomal arrays (Bennink et al., 2001; Brower-Toland et al., 2002; Claudet et al., 2005; Gemmen et al., 2005). The saw tooth pattern at forces larger than ~15 pN indicated the successive disruption of individual nucleosomes (Fig. 5A). On the average, the

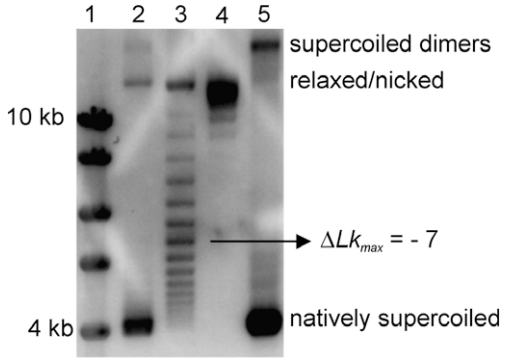

Fig. 4. Control of nucleosome formation by supercoiling activity. The 5197 bp long plasmid pBSα-13 was reconstituted with histones in the presence of Nap-1 at histone octamer: DNA ratios (w/w) of 0.8 (lane 2) and 0.4 (lane 3) and then relaxed with topoisomerasel and deproteinized. Samples were loaded on the agarose gel next a size standard (Smart ladder, Eurogentec, lane 1), the plasmid relaxed in the absence of histones (lane 4) and the natively supercoiled plasmid (lane 5). Fitting a Gaussian distribution to the band intensities in lane 3 yielded a mean number of nucleosomes of 7.6. Doubling the histone concentration (lane 2) yielded full supercoiling. Histones were unable to induce supercoils in the absence of Nap-1 (not shown).

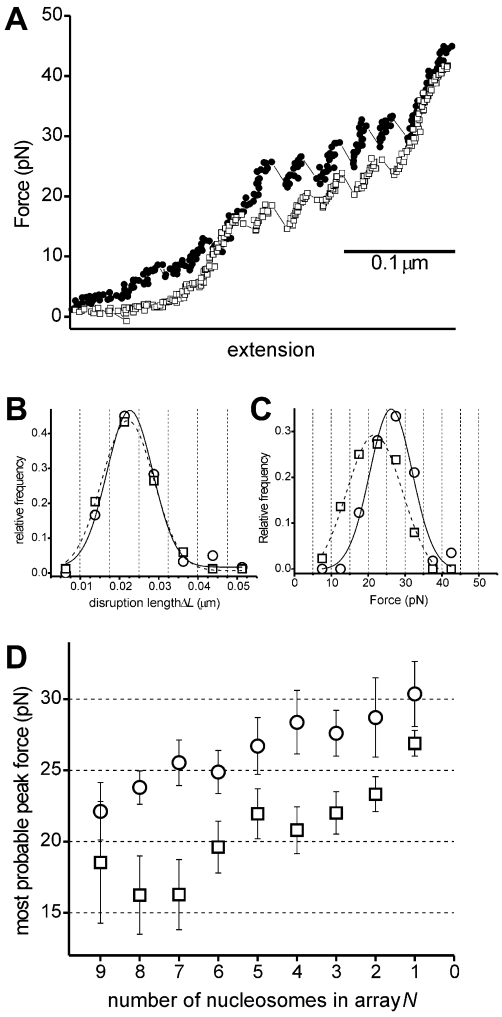

Fig. 5. Force-extension measurements of α-13 (circles) and rand-2 (squares) nucleosomal arrays. Measurements took place at a pulling speed of 50 nm/s. (A) Example force-extension curves. For better visual comparison the curves were shifted along the extension axis so that the naked DNA parts of the curves overlay (this is not exact because of the unequal lengths of the two DNAs). (B) Distribution of disruption lengths and Gaussian fits. These lengths were measured as the distances between linear regression lines through succeeding force peaks as described (Bennink et al., 2001) using a fixed slope determined as the mean of the slopes in each pull. Only data at forces higher than 15 pN were included because here the slopes in the disruption events are the same. (C) Distribution of disruption forces and Gaussian fits. Vertical lines in B and C represent the bins used. (D) Mean disruption forces and standard errors apportioned to the number of nucleosomes N remaining on the tether at each disruption. The number of disruptions was 57 (8 pulls) for α-13 and 88 (14 pulls) for rand-2.

numbers of disruptions agreed quite well with nucleosome numbers determined from the supercoiling method (not shown). Mean disruption lengths, i.e. the DNA length released at each disruption event, were almost equal for both DNAs and measured at 24 (±1 SE) nm for α-13 and 23 (±1 SE) nm for rand-2 (Fig. 5B). This is in good agreement with previous results obtained with different chromatin systems and indicates that the inner nucleosomal winding is released during the disruptions, after release of the outer winding which is released earlier during the initial low force phase (Brower-Toland et al., 2002; Claudet et al., 2005; Gemmen et al., 2005). It also indicates that the amount of DNA wrapped around the histones at the moment of the disruptions was the same on both DNAs.

Disruption forces were determined as the maximum force just before an opening event. The force distributions for both DNAs are

well approximated by a Gaussian function (Fig. 5C). The forces for the AGM–AS nucleosomes are shifted to higher values. Means are 26.4 (±0.7 SE) pN for α-13 and 21.7 (±0.6 SE) pN for rand-2 and are significantly different as calculated in a *t*-test ($p = 4 \times 10^{-6}$, *t*-value (−4.80203)). Forces typically increase with each successive disruption, therefore disruption forces were compared by taking into account the number of nucleosomes *N* present at the moment of each disruption in Fig. 5D. This allows a comparison without force bias by unequal saturation with nucleosomes. Under the simplified assumption that nucleosomes are structurally equal, the probability to disrupt one out of *N* nucleosomes is *N* times the probability for the case that only a single nucleosome is present. In order to number the disruption events, it was assumed that all nucleosomes were disrupted at forces ⩾35 pN and the curves represented naked DNA (Brower-Toland et al., 2005; Gemmen et al., 2005). This was necessary because of the rupturing of the digoxigenin-antidigoxigenin bond before the overstretching plateau. The mean forces apportioned to *N* shown in Fig. 5D clearly reveal consistently higher forces for α-13 for all *N*. The force values for both DNAs show essentially the same trends. The mean difference derived from this plot is 5.8 (±0.6 SE) pN, 1.3 pN higher than the difference between the overall means. Thus, nucleosomes formed on α-13 clearly resisted higher stretching forces.

4. Discussion

In this work, the properties of AGM–AS were studied by gel-electrophoresis, AFM imaging and force-extension measurements using optical tweezers. It is shown that the AS differs from random DNA structurally which is revealed by various measured parameters. Our study additionally suggests that a relatively high nucleosomal stability is a property of AGM–AS chromatin.

AFM revealed reduced end-to-end distances with a derived P_a of 35 nm for the AS 6-mer and the 2-mer. As the 35 nm is unusually low compared with the value of ∼50 nm that is expected for DNA from WLC, it can be concluded that the AS shows a relatively high extent of bending because of the sequence and/or nucleotide composition. A higher extent of bending can be due to a higher bending flexibility or static bending, and it can be a combination of both. Generally, the most significant static contribution in DNA is due to A-tracts with ⩾4 consecutive adenines per tract (Koo et al., 1986; Vologodskaia and Vologodskii, 2002). Fitzgerald et al. (1994) have found by calculating static DNA conformations that the curvature propensity of AGM–AS is not higher than of random sequence DNA on average. Here, the curvature was quantified as the end-ratio, i.e. the ratio of the fragment length to the shortest distance between the ends. A wedge model accounting for A-tract bending was used. The weak gel-retardation, which was even not unambiguously detected in the presence of salt, agrees well with the theoretical calculation but nevertheless indicates a noticeable secondary structure. The AS contains two A-tracts with, respectively, four and five adenines which have nearly the same helical position. An estimate of the influence of these phased A_4–A_5-tracts to the mean end-to-end distance (in thermal equilibrium) is in principle possible using theory developed by Rivetti et al. (1998). This allows to calculate $\langle R^2 \rangle$ of DNA fragments with static bends. In Eq. (18) in their study, $\langle R^2 \rangle$ is a function of the angles of two bends β_1 and β_1, their positions within a DNA fragment and relative orientations specified by the rotation angle ψ. For simplification, we assume that the two phased A_4–A_5-tracts form a single bend at a position centered between them (position 153 in Fig. 1). This allows a calculation for the imaged EcoRI-2-mer (containing the combined bends two times). The angle of the combined bend in each monomer is about 36° (Crothers et al., 1990). The rotation angle depends on the number of helical turns between the bends which would be about 16.5 turns for the monomer length of 172 bp assuming 10.4 bp/turn. For this case, $\psi = 180°$. Since the helical repeat length may depend on the sequence to some degree we consider the two limiting cases that ψ is 180° or 90°. Under these conditions, Eq. (18) in Rivetti et al. yields $\langle R^2 \rangle_{3D}(\beta_1, \beta_1, \psi) = 6530\ \text{nm}^2$ for $P_a = 50$ nm, $\psi = 90°$ and $\langle R^2 \rangle_{3D}(\beta_1, \beta_1, \psi) = 6620\ \text{nm}^2$ for $\psi = 180°$. This is clearly larger than $\langle R^2 \rangle_{3D} = 5830\ \text{nm}^2$ corresponding with $P_a = 35$ nm (Eq. (1)). Although the assumed configuration cannot be understood as a sufficient model for the entire AS sequence, this gives an estimate that the A_4–A_5-tracts cannot fully account for the reduced end-to-distances. The end-to-end distances of the monomer length segments isolated from the imaged 2-mer did also not indicate that the region with the A_4–A_5-tracts is solely responsible for the reduced end-to-end distances. We denote the persistence length value corrected for the influence by the phased A_4–A_5-tracts as $P_{a\Delta A4/5}$. For the assumptions made here, Eq. (18) in Rivetti et al. yields $P_{a\Delta A4/5} = 41$ nm ($\psi = 90°$) and 40 nm ($\psi = 180°$) for the measured $\langle R^2 \rangle_{2D}$. According to this estimation, the persistence length of the entire sequence is still much shorter than of random DNA. The remaining A_3-tracts and AATT (positions 32 and 94) may have an additional influence. However, A_3-tracts, even when periodically arranged, do not cause an appreciable gel-migration anomaly (Diekmann, 1986; Koo et al., 1986). Also, the remaining A-tracts are not arranged in a helical phase but an eight to nine bp periodicity is found between positions 159 and 15. An additional explanation is an increased bending flexibility. A relatively high A/T content, which is 57% in AGM–AS, can be associated with an increased static bending as well as an increased flexibility. Regions with the highest bending flexibility in a heterogeneous DNA sequence correlated with local A/T content, as measured by AFM (Scipioni et al., 2002). Our control DNAs has a lower A/T content (53% for rand-1 and 50% for rand-2) than the AS. An identifiable sequence-dependent contribution to an increased bending flexibility is given by clustered CA/TG steps (marked red in Fig. 1). CA/TG is structurally highly polymorphic based on crystallography (El Hassan and Calladine, 1997; Neugebauerova and Kypr, 2000) and exhibits relatively low base stacking interactions (Protozanova et al., 2004). It enhanced the circularization of DNA fragments increasingly in the order CA < CAC < CACA suggesting a high susceptibility toward conformational fluctuations in elongated CA/TG (Lyubchenko et al., 1993). Four CACA/TGTG blocks occur per monomer, which is more than the expected average occurrence of 1.3 (±1.1 SD) per 172 bp in random DNA ($2 \times 0.25^4 \times 169$). The TA step (underlined in Fig. 1) which is characterized by even lower base stacking interactions (Protozanova et al., 2004) and ranked highly deformable based on crystallography (El Hassan and Calladine, 1997; Neugebauerova and Kypr, 2000) is not particularly frequent (six times). A large accumulation of CA/TG steps is characteristic of some of the sequences that were selected on the basis of their high equilibrium affinity for nucleosome formation in mouse (Widlund et al., 1997). In total, a number of different sequence types which share the ability to form stable nucleosomes, including A-tract rich satellite DNA, were identified in this work. Interestingly, all these sequences were found to localize to the centromeres. Reduced P_a was measured for sequences from this set that contain elongated runs of alternating CA/TG (45 nm) or CAG/CTG (42 nm) by AFM (Virstedt et al., 2004). It is conceivable that CA/TG is relevant for nucleosome formation in the AS. A region rich in alternating CA/TG (positions 21 to 44 in Fig. 1) is found in the central part of the major nucleosomal binding site whose center is at position 43 (Neubauer et al., 1986).

As an additional structural parameter, the naked AS showed a higher susceptibility towards extension. The overstretching transition force was 18% smaller than observed for the control DNA. Again, the AT-content and the occurrence of A-tracts can explain this observation (Leger et al., 1998; Rief et al., 1999). An additional

influence could be given by the CA/TG steps because of relatively low base stacking interactions. An about 10% difference in the transition force was observed for two several kb long sequences with 50% and 70% A/T by Leger et al. (1998). This suggests that the 18% smaller transition force for the AS is not only due to the nucleotide composition but also the sequence. Like a higher bending flexibility, the overstretching force potentially indicates a biologically relevant property, although it is induced by high stretching forces (Leger et al., 1998): the energy change between B-form and the overstretched state per bp is low enough ($\sim$3 kT) that local structural distortions of the B-DNA conformation can occur spontaneously by thermal fluctuations. Therefore, a lower transition force may indicate mechanical properties that can play a role in DNA–protein complex formation. The other observation from the force measurements were higher forces associated with straightening the naked AS. This is in qualitative agreement with reduced end-to-end distances observed by AFM. This shows that the conformational properties of the AS affect the forces under extension noticeably relative to random DNA. However, applying WLC to the AFM data and the force-extension data yielded different results for this DNA. The value of P_a derived from the force-extension data was only 18 nm which demonstrates that WLC cannot describe the bending behavior of the AS. A theory accounting for its force-extension behavior, which is currently not available, needs to consider different possible factors such as the effect of local intrinsic bends and/or sites of increased deformability and their position dependent interaction under tension. The relation of structural disorder in DNA to the apparent persistence length under tension has been studied theoretically considering local (protein induced) kinks or loops (Yan and Marko, 2003, 2004; Kulic et al., 2007). As well important could be force induced twist deformations (Gore et al., 2006).

Considering only DNA and histones, satellite DNA may promote the structural stability and compactness of chromatin by forming regularly spaced as well as structurally stable nucleosomes (Widlund et al., 1997; Gilbert and Allan, 2001; Segal et al., 2006). In our stretching experiments of nucleosomal arrays, markedly higher disruption forces were observed for nucleosomes reconstituted with α-13 as compared with those reconstituted with rand-2. The mean difference was 5.8 pN (on average $\sim$30% the values measured for rand-2 for each N, see Fig. 5). Rand-2, as a non-eukaryotic DNA, does not contain any evolved nucleosome binding signals. Yet, the mean force of 21.7 pN is rather comparable to the forces observed at the same salt conditions for isolated chicken chromatin (19.6 pN) and somewhat higher than observed for nucleosomes reconstituted with 5S rDNA using the salt dialysis method (17.6 pN) (Claudet et al., 2005). The range of forces between $\sim$10 and 35 pN corresponds with the cited work and the measurements were done at similar pulling speeds. The higher forces for α-13 reveal that the nucleosomes are structurally more stable. Forces may additionally differ because of a more regular nucleosomal arrangement expected for α-13. In previous studies, disruptions were interpreted in terms of the response of isolated nucleosomes towards stretching forces because of the specific unfolding mechanism of nucleosomal arrays (Bennink et al., 2001; Brower-Toland et al., 2002, 2005; Gemmen et al., 2005). The fiber is near its full extension at the moment of the disruptions (Brower-Toland et al., 2002). Therefore, internucleosomal interactions and the linear nucleosomal arrangement along the DNA likely have a minor influence. No dependency of the mean disruption force per pull on the number of observed events was apparent and also the loading rates in the force peaks did not differ between the DNAs on average (not shown). The mean disruption lengths were the same for both DNAs. Thus, although some uncertainty remains in the interpretation of the force measurements because of a potential influence due to the nucleosomal arrangement, it is very likely that the higher disruption forces show a sequence-induced stability of the nucleosomes. Further work is required to find out how disruption forces relate to equilibrium affinities and which sequence properties account for the higher resistance towards stretching forces. Reconstitution experiments with modified AGM–AS fragments indicated that sequence-dependent DNA–histone interactions are established along the full length of the major nucleosomal binding site (Neubauer et al., 1986). Here, we can conclude that the AS seems to give another example for a sequence which stably interacts with histones and which also shows distinct overall bending properties (Widlund et al., 1999; Cloutier and Widom, 2004; Virstedt et al., 2004).

In summary, the findings reveal that AGM–AS offers structural properties that are distinct from bulk DNA. The AS showed clearly different bending properties, a higher susceptibility towards extension and relatively high nucleosomal disruption forces. This supports the idea that structural properties of satellite DNA are involved in the centromeric heterochromatin formation. In AGM, a structural function of the AS sequence could relate to the homogenous monomeric composition of the satellite arrays. Offering a well-structured and rigid platform for the kinetochore assembly and the microtubule attachment is an expected function of the centromeric heterochromatin. Also, it has been proposed that the structural properties of heterochromatin are important to maintain the centromere position (Dalal et al., 2007). A high resistance of the chromatin complex towards stretching forces could be important during chromosome alignment and segregation. Therefore, condensation of the chromatin due to nucleosomal phasing together with a high structural stability of the nucleosomes could be advantageous. Like mouse, yeast gives another known example of forming stable nucleosomes at centromeres (Segal et al., 2006).

Acknowledgments

We are grateful to Chandrashekhar Murade, Kirsten van Leijenhorst-Groener, Juergen Huisstede and Kees van der Werf for technical support. Thanks to Norbert Muecke for discussions about AFM and Vinod Subramaniam for helpful comments. We thank Gabriele Mueller and Waldemar Waldeck for their support with the isolation and cloning of satellites which was done previously in the laboratory of Jörg Langowski.

Appendix A. Supplementary data

Supplementary data associated with this article can be found, in the online version, at doi:10.1016/j.jsb.2009.03.010.

References

Alexandrov, I., Kazakov, A., Tumeneva, I., Shepelev, V., Yurov, Y., 2001. Alpha-satellite DNA of primates: old and new families. Chromosoma 110 (4), 253–266.
Amor, D.J., Choo, K.H., 2002. Neocentromeres: role in human disease, evolution, and centromere study. Am. J. Hum. Genet. 71 (4), 695–714.
Baumann, C.G., Smith, S.B., Bloomfield, V.A., Bustamante, C., 1997. Ionic effects on the elasticity of single DNA molecules. Proc. Natl. Acad. Sci. USA 94 (12), 6185–6190.
Bednar, J., Furrer, P., Katritch, V., Stasiak, A.Z., Dubochet, J., Stasiak, A., 1995. Determination of DNA persistence length by cryo-electron microscopy. Separation of the static and dynamic contributions to the apparent persistence length of DNA. J. Mol. Biol. 254 (4), 579–594.
Bennink, M.L., Leuba, S.H., Leno, G.H., Zlatanova, J., de Grooth, B.G., Greve, J., 2001. Unfolding individual nucleosomes by stretching single chromatin fibers with optical tweezers. Nat. Struct. Biol. 8 (7), 606–610.
Brower-Toland, B., Wacker, D.A., Fulbright, R.M., Lis, J.T., Kraus, W.L., Wang, M.D., 2005. Specific contributions of histone tails and their acetylation to the mechanical stability of nucleosomes. J. Mol. Biol. 346 (1), 135–146.
Brower-Toland, B.D., Smith, C.L., Yeh, R.C., Lis, J.T., Peterson, C.L., Wang, M.D., 2002. Mechanical disruption of individual nucleosomes reveals a reversible multistage release of DNA. Proc. Natl. Acad. Sci. USA 99 (4), 1960–1965.
Bussiek, M., Mucke, N., Langowski, J., 2003. Polylysine-coated mica can be used to observe systematic changes in the supercoiled DNA conformation by scanning force microscopy in solution. Nucleic Acids Res. 31 (22), e137.

Bussiek, M., Muller, G., Waldeck, W., Diekmann, S., Langowski, J., 2007. Organisation of nucleosomal arrays reconstituted with repetitive African green monkey alpha-satellite DNA as analysed by atomic force microscopy. Eur. Biophys. J. 37 (1), 81–93.

Canapa, A., Cerioni, P.N., Barucca, M., Olmo, E., Caputo, V., 2002. A centromeric satellite DNA may be involved in heterochromatin compactness in gobiid fishes. Chromosome Res. 10 (4), 297–304.

Claudet, C., Angelov, D., Bouvet, P., Dimitrov, S., Bednar, J., 2005. Histone octamer instability under single molecule experiment conditions. J. Biol. Chem. 280 (20), 19958–19965.

Cloutier, T.E., Widom, J., 2004. Spontaneous sharp bending of double-stranded DNA. Mol. Cell 14 (3), 355–362.

Cluzel, P., Lebrun, A., Heller, C., Lavery, R., Viovy, J.L., Chatenay, D., Caron, F., 1996. DNA: an extensible molecule. Science 271 (5250), 792–794.

Conde e Silva, N., Black, B.E., Sivolob, A., Filipski, J., Cleveland, D.W., Prunell, A., 2007. CENP-A-containing nucleosomes: easier disassembly versus exclusive centromeric localization. J. Mol. Biol. 370 (3), 555–573.

Crothers, D.M., Haran, T.E., Nadeau, J.G., 1990. Intrinsically bent DNA. J. Biol. Chem. 265 (13), 7093–7096.

Cui, Y., Bustamante, C., 2000. Pulling a single chromatin fiber reveals the forces that maintain its higher-order structure. Proc. Natl. Acad. Sci. USA 97 (1), 127–132.

Dalal, Y., Wang, H., Lindsay, S., Henikoff, S., 2007. Tetrameric structure of centromeric nucleosomes in interphase *Drosophila* cells. PLoS Biol. 5 (8), e218.

Diekmann, S., 1987. Temperature and salt dependence of the gel migration anomaly of curved DNA fragments. Nucleic Acids Res. 15 (1), 247–265.

Diekmann, S., 1986. Sequence specificity of curved DNA. FEBS Lett. 195 (1–2), 53–56.

Du, Q., Smith, C., Shiffeldrim, N., Vologodskaia, M., Vologodskii, A., 2005. Cyclization of short DNA fragments and bending fluctuations of the double helix. Proc. Natl. Acad. Sci. USA 102 (15), 5397–5402.

El Hassan, M.A., Calladine, C.R., 1997. Conformational characteristics of DNA: empirical classifications and a hypothesis for the conformational behaviour of dinucleotide steps. Trans. R. Soc. Lond. A355, 43–100.

Fitzgerald, D.J., Dryden, G.L., Bronson, E.C., Williams, J.S., Anderson, J.N., 1994. Conserved patterns of bending in satellite and nucleosome positioning DNA. J. Biol. Chem. 269 (33), 21303–21314.

Folco, H.D., Pidoux, A.L., Urano, T., Allshire, R.C., 2008. Heterochromatin and RNAi are required to establish CENP-A chromatin at centromeres. Science 319 (5859), 94–97.

Gemmen, G.J., Sim, R., Haushalter, K.A., Ke, P.C., Kadonaga, J.T., Smith, D.E., 2005. Forced unraveling of nucleosomes assembled on heterogeneous DNA using core histones, NAP-1, and ACF. J. Mol. Biol. 351 (1), 89–99.

Gilbert, N., Allan, J., 2001. Distinctive higher-order chromatin structure at mammalian centromeres. Proc. Natl. Acad. Sci. USA 98 (21), 11949–11954.

Gittes, F., Schmidt, C.F., 1998. Signals and noise in micromechanical measurements. Methods Cell Biol. 55, 129–156.

Goldberg, I.G., Sawhney, H., Pluta, A.F., Warburton, P.E., Earnshaw, W.C., 1996. Surprising deficiency of CENP-B binding sites in African green monkey alpha-satellite DNA: implications for CENP-B function at centromeres. Mol. Cell. Biol. 16 (9), 5156–5168.

Gore, J., Bryant, Z., Nollmann, M., Le, M.U., Cozzarelli, N.R., Bustamante, C., 2006. DNA overwinds when stretched. Nature 442 (7104), 836–839.

Harrington, J.J., Van Bokkelen, G., Mays, R.W., Gustashaw, K., Willard, H.F., 1997. Formation of de novo centromeres and construction of first-generation human artificial microchromosomes. Nat. Genet. 15 (4), 345–355.

Henikoff, S., Dalal, Y., 2005. Centromeric chromatin: what makes it unique? Curr. Opin. Genet. Dev. 15 (2), 177–184.

Hoischen, C., Bolshoy, A., Gerdes, K., Diekmann, S., 2004. Centromere parC of plasmid R1 is curved. Nucleic Acids Res. 32 (19), 5907–5915.

Huisstede, J.H., van Rooijen, B.D., van der Werf, K.O., Bennink, M.L., Subramaniam, V., 2006. Dependence of silicon position-detector bandwidth on wavelength, power, and bias. Opt. Lett. 31 (5), 610–612.

Koo, H.S., Crothers, D.M., 1988. Calibration of DNA curvature and a unified description of sequence-directed bending. Proc. Natl. Acad. Sci. USA 85 (6), 1763–1767.

Koo, H.S., Wu, H.M., Crothers, D.M., 1986. DNA bending at adenine, thymine tracts. Nature 320 (6062), 501–506.

Kulic, I.M., Mohrbach, H., Thaokar, R., Schiessel, H., 2007. Equation of state of looped DNA. Phys. Rev. E Stat. Nonlin. Soft Matter Phys. 75 (1 Pt 1), 011913.

Leger, J.F., Robert, J., Bourdieu, L., Chatenay, D., Marko, J.F., 1998. RecA binding to a single double-stranded DNA molecule: a possible role of DNA conformational fluctuations. Proc. Natl. Acad. Sci. USA 95 (21), 12295–12299.

Leuba, S.H., Karymov, M.A., Tomschik, M., Ramjit, R., Smith, P., Zlatanova, J., 2003. Assembly of single chromatin fibers depends on the tension in the DNA molecule: magnetic tweezers study. Proc. Natl. Acad. Sci. USA 100 (2), 495–500.

Luger, K., Mader, A.W., Richmond, R.K., Sargent, D.F., Richmond, T.J., 1997. Crystal structure of the nucleosome core particle at 2.8 Å resolution. Nature 389 (6648), 251–260.

Lyubchenko, Y.L., Shlyakhtenko, L.S., Appella, E., Harrington, R.E., 1993. CA runs increase DNA flexibility in the complex of lambda Cro protein with the OR3 site. Biochemistry 32 (15), 4121–4127.

Marko, J.F., Siggia, E.D., 1995. Stretching DNA. Macromolecules 28, 8759–8770.

Martinez-Balbas, A., Rodriguez-Campos, A., Garcia-Ramirez, M., Sainz, J., Carrera, P., Aymami, J., Azorin, F., 1990. Satellite DNAs contain sequences that induced curvature. Biochemistry 29 (9), 2342–2348.

McQuibban, G.A., Commisso-Cappelli, C.N., Lewis, P.N., 1998. Assembly, remodeling, and histone binding capabilities of yeast nucleosome assembly protein 1. J. Biol. Chem. 273 (11), 6582–6590.

Mihardja, S., Spakowitz, A.J., Zhang, Y., Bustamante, C., 2006. Effect of force on mononucleosomal dynamics. Proc. Natl. Acad. Sci. USA 103 (43), 15871–15876.

Moreno-Herrero, F., Seidel, R., Johnson, S.M., Fire, A., Dekker, N.H., 2006. Structural analysis of hyperperiodic DNA from *Caenorhabditis elegans*. Nucleic Acids Res. 34 (10), 3057–3066.

Mucke, N., Kreplak, L., Kirmse, R., Wedig, T., Herrmann, H., Aebi, U., Langowski, J., 2004. Assessing the flexibility of intermediate filaments by atomic force microscopy. J. Mol. Biol. 335 (5), 1241–1250.

Neubauer, B., Linxweiler, W., Horz, W., 1986. DNA engineering shows that nucleosome phasing on the African green monkey alpha-satellite is the result of multiple additive histone-DNA interactions. J. Mol. Biol. 190 (4), 639–645.

Neugebauerova, S., Kypr, J., 2000. Invariant and variable base stacking geometries in B-DNA and A-DNA. J. Biomol. Struct. Dyn. 18 (1), 73–81.

Odijk, T., 1995. Stiff chains and filaments under tension. Macromolecules (28), 716–718.

Okada, T., Ohzeki, J., Nakano, M., Yoda, K., Brinkley, W.R., Larionov, V., Masumoto, H., 2007. CENP-B controls centromere formation depending on the chromatin context. Cell 131 (7), 1287–1300.

Protozanova, E., Yakovchuk, P., Frank-Kamenetskii, M.D., 2004. Stacked-unstacked equilibrium at the nick site of DNA. J. Mol. Biol. 342 (3), 775–785.

Rief, M., Clausen-Schaumann, H., Gaub, H.E., 1999. Sequence-dependent mechanics of single DNA molecules. Nat. Struct. Biol. 6 (4), 346–349.

Rivetti, C., Guthold, M., Bustamante, C., 1996. Scanning force microscopy of DNA deposited onto mica: equilibration versus kinetic trapping studied by statistical polymer chain analysis. J. Mol. Biol. 264 (5), 919–932.

Rivetti, C., Walker, C., Bustamante, C., 1998. Polymer chain statistics and conformational analysis of DNA molecules with bends or sections of different flexibility. J. Mol. Biol. 280 (1), 41–59.

Rosenberg, H., Singer, M., Rosenberg, M., 1978. Highly reiterated sequences of SIMIANSIMIANSIMIANSIMIANSIMIAN. Science 200 (4340), 394–402.

Scipioni, A., Anselmi, C., Zuccheri, G., Samori, B., De Santis, P., 2002. Sequence-dependent DNA curvature and flexibility from scanning force microscopy images. Biophys. J. 83 (5), 2408–2418.

Segal, E., Fondufe-Mittendorf, Y., Chen, L., Thastrom, A., Field, Y., Moore, I.K., Wang, J.P., Widom, J., 2006. A genomic code for nucleosome positioning. Nature 442 (7104), 772–778.

Shrader, T.E., Crothers, D.M., 1990. Effects of DNA sequence and histone-histone interactions on nucleosome placement. J. Mol. Biol. 216 (1), 69–84.

Simon, R.H., Felsenfeld, G., 1979. A new procedure for purifying histone pairs H2A + H2B and H3 + H4 from chromatin using hydroxylapatite. Nucleic Acids Res. 6 (2), 689–696.

Smith, S.B., Cui, Y., Bustamante, C., 1996. Overstretching B-DNA: the elastic response of individual double-stranded and single-stranded DNA molecules. Science 271 (5250), 795–799.

Strick, T.R., Allemand, J.F., Bensimon, D., Bensimon, A., Croquette, V., 1996. The elasticity of a single supercoiled DNA molecule. Science 271 (5257), 1835–1837.

Tanaka, Y., Tachiwana, H., Yoda, K., Masumoto, H., Okazaki, T., Kurumizaka, H., Yokoyama, S., 2005. Human centromere protein B induces translational positioning of nucleosomes on alpha-satellite sequences. J. Biol. Chem. 280 (50), 41609–41618.

Tolstorukov, M.Y., Colasanti, A.V., McCandlish, D.M., Olson, W.K., Zhurkin, V.B., 2007. A novel roll-and-slide mechanism of DNA folding in chromatin: implications for nucleosome positioning. J. Mol. Biol. 371 (3), 725–738.

Travers, A.A., 2004. The structural basis of DNA flexibility. Philos. Transact. A Math. Phys. Eng. Sci. 362 (1820), 1423–1438.

Trifonov, E.N., Sussman, J.L., 1980. The pitch of chromatin DNA is reflected in its nucleotide sequence. Proc. Natl. Acad. Sci. USA 77 (7), 3816–3820.

Van der Werf, K., Putman, C.J., De Grooth, B.G., Segerink, F.B., Schipper, E.H., van Hulst, N.F., Greve, J., 1993. Compact stand-alone atomic force microscope. Rev. Sci. Intrument. 64, 2892–2897.

Virstedt, J., Berge, T., Henderson, R.M., Waring, M.J., Travers, A.A., 2004. The influence of DNA stiffness upon nucleosome formation. J. Struct. Biol. 148 (1), 66–85.

Vologodskaia, M., Vologodskii, A., 2002. Contribution of the intrinsic curvature to measured DNA persistence length. J. Mol. Biol. 317 (2), 205–213.

Wagner, G., Bancaud, A., Quivy, J.P., Clapier, C., Almouzni, G., Viovy, J.L., 2005. Compaction kinetics on single DNAs: purified nucleosome reconstitution systems versus crude extract. Biophys. J. 89 (5), 3647–3659.

Wang, M.D., Yin, H., Landick, R., Gelles, J., Block, S.M., 1997. Stretching DNA with optical tweezers. Biophys. J. 72 (3), 1335–1346.

Widlund, H.R., Cao, H., Simonsson, S., Magnusson, E., Simonsson, T., Nielsen, P.E., Kahn, J.D., Crothers, D.M., Kubista, M., 1997. Identification and characterization of genomic nucleosome-positioning sequences. J. Mol. Biol. 267 (4), 807–817.

Widlund, H.R., Kuduvalli, P.N., Bengtsson, M., Cao, H., Tullius, T.D., Kubista, M., 1999. Nucleosome structural features and intrinsic properties of the TATAAACGCC repeat sequence. J. Biol. Chem. 274 (45), 31847–34852.

Widom, J., 2001. Role of DNA sequence in nucleosome stability and dynamics. Q. Rev. Biophys. 34 (3), 269–324.

Yan, J., Marko, J.F., 2003. Effects of DNA-distorting proteins on DNA elastic response. Phys. Rev. E Stat. Nonlin. Soft Matter Phys. 68 (1 Pt 1), 011905.

Yan, J., Marko, J.F., 2004. Localized single-stranded bubble mechanism for cyclization of short double helix DNA. Phys. Rev. Lett. 93 (10), 108108.